Optimum Cell Size for High Order Singular Basis Functions At Geometric Corners

[1]M. M. Bibby, [1]A. F. Peterson, and [2]C. M. Coldwell

[1]School of ECE, Georgia Institute of Technology, Atlanta, GA 30332,
mbibby@ece.gatech.edu, peterson@ece.gatech.edu

[2]Red Hat Inc., 10 Technology Park Drive, Westford, MA 01886,
coldwell@frank.harvard.edu

Abstract – Both low-order and high-order singular basis functions have been previously proposed for modeling edge singularities in the current and charge densities at geometric corners in electromagnetic integral equation formulations. This paper attempts to identify an optimum dimension for the cells adjacent to corners, as a function of the polynomial degree of the representation used away from the corner cells. The residual error obtained via the solution of an over-determined system of equations is used to judge the relative accuracy of various approaches.

Keywords: boundary element method, corner singularity, edge condition, high order basis functions, method of moments, over-determined systems, residual error, singular basis functions.

I. INTRODUCTION

For several decades, most numerical procedures for solving the integral equations for electromagnetic field problems have been based on low-order methods, where the representation of the primary unknown is in terms of constant or linear polynomials, and the convergence rates are often no faster than O(h^2), where h is the characteristic cell dimension associated with the numerical model. Higher order methods have been shown to provide a better trade-off between high accuracy and improved computational efficiency than low-order methods. However, many practical structures contain corners or edges, where the charge density or current density may exhibit a singularity. In the absence of an explicit attempt to incorporate the actual singularity into the representation for the unknown quantity, the accuracy improvements offered by high order basis functions are negated. A number of authors have proposed singular basis functions [1-5], including the possibility of incorporating multiple singular terms to provide high order behavior [6-7].

Reference [7] proposed a methodology for high order modeling of edge singularities in two-dimensional problems. In cells not adjacent to corners or edges, a complete polynomial representation was employed up to order q, or degree q–1. In cells adjacent to corners, this representation was augmented with approximately (q+1)/2 additional, singular terms. The singular terms were obtained from the asymptotic series for the current density near the tip of the appropriate infinite wedge [8]. However, the work reported in reference [7] only considered the case where the cells adjacent to the corners were of the same dimension as the other cells used throughout the model.

In the following, the investigation of [7] is extended to consider the relative cell size of the corner cells, in an attempt to optimize the overall computational efficiency. The number of additional singular terms used in the corner cells and the corner cell dimension are permitted to vary, while local and global error levels are monitored. Results show that the accuracy in the corner cells improves as additional singular terms are included, and as the corner cell dimension is reduced. However, if the corner cell dimension is made too small, the accuracy degrades in the cell adjacent to the corner cell. Until this limit is reached, an optimum balance between the error in the corner cells and the non-corner cells is achieved when the number of singular terms is approximately equal to q and the corner cell size is roughly twice that of the non-corner cells.

II. SINGULAR BASIS FUNCTIONS FOR CORNER CELLS

A solution for the surface current density on an infinite wedge is developed in [8]. Based on those results, a general asymptotic expression for the current density as a function of ρ on the face of the wedge, near the tip (ρ = 0), can be written for the transverse magnetic (TM)-to-z case as,

$$J_z : \sum_{m=0}^{\infty}\sum_{n=1}^{\infty} c_{mn}\rho^{2m+\upsilon_n-1} \quad (1)$$

where a cylindrical coordinate system (ρ, ϕ, z) is employed in equation (1),

$$\upsilon_n = \frac{n\pi}{(2\pi - \alpha)}, \quad n = 1,\ 2,\ 3,\ \ldots \tag{2}$$

A similar expression for the transverse electric (TE)-to-*z* case is,

$$J_\rho : \sum_{m=0}^{\infty}\sum_{n=0}^{\infty} d_{mn}\rho^{2m+\upsilon_n} \tag{3}$$

where υ_n is defined as,

$$\upsilon_n = \frac{n\pi}{(2\pi - \alpha)}, \quad n = 0,\ 1,\ 2,\ \ldots \tag{4}$$

Reference [7] proposed a hierarchical family of basis functions for use in cells adjacent to geometric corners. For cells that are not adjacent to a corner of the contour, a Legendre expansion of order q is employed. In the corner cells, the same representation is augmented by including some number of terms with non-integer exponents from equation (1) or equation (3).

As an illustration, consider the representation used in the cell adjacent to a 90 degree corner. The exponents arising from the expansion in equation (1) can be arranged in a sequence,

$$\left\{-\frac{1}{3},\ \frac{1}{3},\ 1,\ \frac{5}{3},\ \frac{7}{3},\ 3,\ \frac{11}{3},\ \ldots\right\}$$

Table 1 illustrates the specific exponents that would be included in an "order q" representation for two different approaches. In the first, $[(q+1)/2]$ singular terms are included in the expansion, where the square brackets denote the greatest integer. In the second approach, q singular terms are incorporated. In either case orthogonal hierarchical basis functions are constructed from the set of exponents in Table 1, using a Gram-Schmidt procedure as described in [7]. For the case of q = 3, and N_{sing} = $[(q+1)/2]$, the representation at a 90° corner involves 5 basis functions, constructed from terms of the form,

$$\left\{u^{-1/3},\ 1,\ u^{1/3},\ u,\ u^2\right\}$$

As another example, the expansion functions for a 60° corner were previously given in [7].

While [7] concluded that approximately $(q+1)/2$ singular terms were required in corner cells to produce higher order behavior and accuracy comparable to that in non-corner cells, that conclusion was limited to the case where the corner cells were the same size as the non-corner cells. In the present investigation, the optimum number of singular terms is considered as the corner cell dimensions are varied relative to the non-corner cells.

Table 1. Exponents used in the representation for TM current density in the case of a 90 degree angle, as a function of the order q and the parameter N_{sing}.

q	Regular exponents	Singular exponents when $N_{sing}=[(q+1)/2]$	Singular exponents when $N_{sing} = q$
1	0	–1/3	–1/3
2	0, 1	–1/3	–1/3, 1/3
3	0, 1, 2	–1/3, 1/3	–1/3, 1/3, 5/3
4	0, 1, 2, 3	–1/3, 1/3	–1/3, 1/3, 5/3, 7/3

III. DEFINITIONS

A specific representation of the surface current density will involve some number of unknown coefficients that must be determined. We refer to that as the number of *degrees of freedom* (DoF) in the expansion. As indicated above, non-corner cells will employ an expansion of order q, meaning q degrees of freedom per cell. Corner cells will employ N_{sing} additional terms, for a total of $(q + N_{sing})$ degrees of freedom per cell. Our expansions do not straddle adjacent cells or impose cell-to-cell continuity.

Numerical results will be obtained using the electric-field integral equation (EFIE) and the magnetic field integral equation (MFIE). These equations and the method of moments numerical solution procedure are described in [9]. For the present investigation, a weighted point-matching procedure is used to enforce the integral equations. The procedure uses an over-determined system of equations obtained by employing twice as many testing points within each cell (m = 2) as there are unknowns to be determined in that cell. Thus, a cell with q expansion functions produces mq equations. The equations are obtained at nodes of a Gauss-Legendre quadrature rule and weighted by the square root of quadrature weights, and the resulting numerical solution minimizes the integrated square error of the residual on the scatterer surface [10-11]. The primary motivation for the use of an over-determined system is that, as a byproduct of the least-square solution algorithm, we obtain the local residual error at each test point. The residual error associated with the integral equation is used to assess the relative accuracy of each numerical result.

The residual error is scaled by the excitation to produce the normalized residual error (*NRE*). For instance, the *NRE* is expressed for the TM-to-z EFIE on a perfectly conducting scatterer as,

$$NRE = \frac{\sqrt{\int\left|E_z^{inc} - E_z^s\right|^2 dt}}{\sqrt{\int\left|E_z^{inc}\right|^2 dt}} \cong \frac{\sqrt{\sum_{i=1}^{N_{tp}} w_i \left|E_z^{inc}(t_i) - E_z^s(t_i)\right|^2}}{\sqrt{\sum_{i=1}^{N_{tp}} w_i \left|E_z^{inc}(t_i)\right|^2}} \tag{5}$$

where $\{t_i\}$ and $\{w_i\}$ denote Gauss-Legendre quadrature nodes and weights. N_{tp} is the total number of points included in the measure. To provide a local error estimate, equation (5) is computed for each cell with N_{tp} equal to the number of test points within that cell. The number of test points in a corner cell is usually different from the number of test points in cells not adjacent to a corner. To obtain a global error estimate, equation (5) is computed for the entire problem domain with N_{tp} = m(DoF). For the other integral equations considered, equation (5) is modified in an obvious way to implement the appropriate residual.

The rate at which the global *NRE* decreases as a function of cell size or number of unknowns can be used to judge the extent to which high order behavior is exhibited by the results. Consider two results, the first yielding NRE_1 with N_1 unknowns, and the second exhibiting NRE_2 with N_2 unknowns. The incremental slope of the associated error curve may be obtained from successive results using [12],

$$Slope_q = \frac{\log_{10}(NRE_2) - \log_{10}(NRE_1)}{\log_{10}(N_2) - \log_{10}(N_1)} \qquad (6)$$

where the subscript serves as a reminder that the principal expansions are of order q. For smooth scatterers, values of equation (6) often approximate integers as N increases.

The *edge cell size ratio* (ECSR) will be used to denote the ratio of the dimension of the corner cells to that of the non-corner cells. In the following, all non-corner cells will be maintained at a common dimension, while all corner cells are scaled from that dimension by the factor ECSR.

IV. RESULTS FOR ECSR = 1

In a previous work by the authors with high order representations [12], circular cylinders were considered since they offer exact analytical solutions. To establish a baseline for reference, Figs. 1(a) and 1(b) show the global *NRE* and $Slope_q$ versus the degrees of freedom for a circular cylinder of 12 λ circumference, where λ is the wavelength. These plots illustrate uniform *h*-refinement (shrinking all the cells in unison for a fixed degree representation). These data were obtained from a solution of the MFIE for the TM polarization, using Legendre polynomial representations for the current density, and models employing equal-sized curved cells.

The data in Fig. 1 clearly exhibit higher order behavior, and the $Slope_q$ values approximate integers as the discretizations are refined. A general goal of higher-order representations for problems with edges or corners is to achieve similar behavior. Figures 2(a) and 2(b) show plots of the global *NRE* and $Slope_q$ versus the degrees of freedom for a cylinder of triangular cross section shape, and a total periphery of 12 λ.

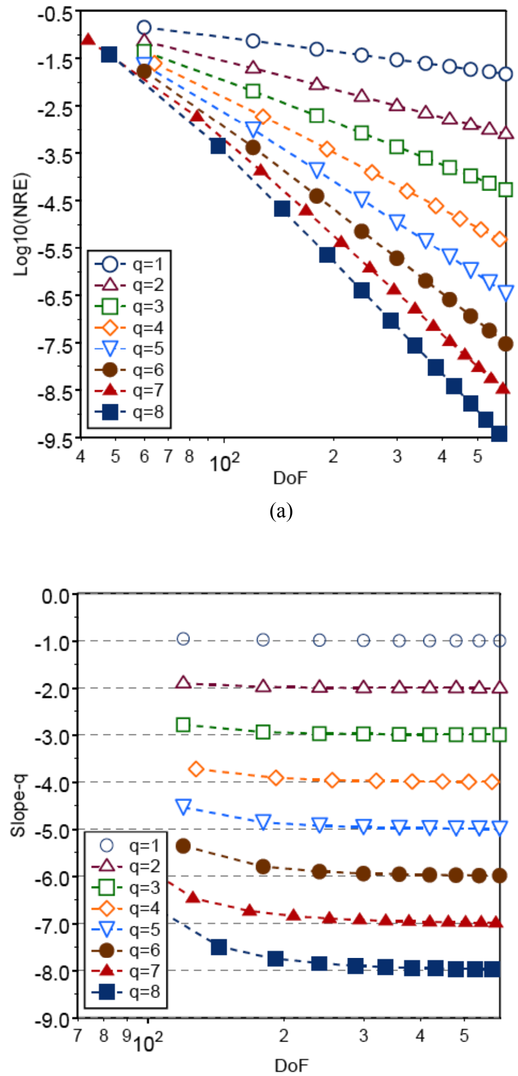

(a)

(b)

Fig. 1. (a) Global *NRE* values and (b) $Slope_q$ values for the TM MFIE solutions for a circular cylinder of 12 λ circumference, when illuminated by a uniform plane. wave. Uniform cell sizes were used with a Legendre polynomial representation of order q.

Results in Fig. 2 were obtained from the TM MFIE. Corner cells have the same dimension as non-corner cells (ECSR = 1). In this situation, Legendre polynomial representations of order q are used in non-corner cells, while corner cells employ an additional N_{sing}=[(q + 1)/2] singular terms, where the square bracket denotes greatest integer. As the number of degrees of freedom increases, the *NRE* curves in Fig. 2(a) level off, and the global results do not appear to produce high order convergence. This is reflected in the $Slope_q$ curves in Fig. 2(b).

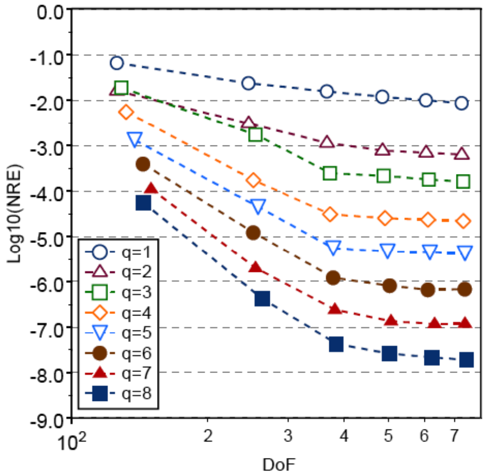

(a)

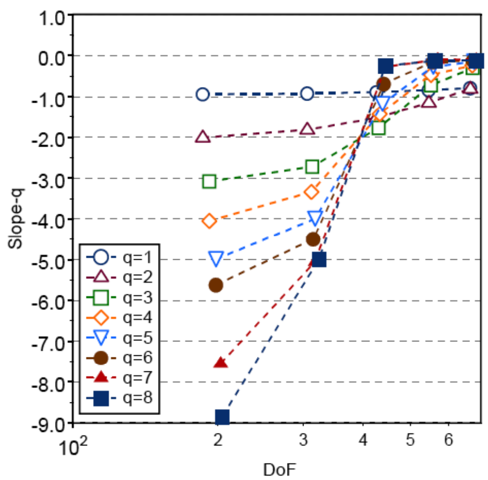

(b)

Fig. 2. (a) Global *NRE* values and (b) $Slope_q$ values for the TM MFIE solutions for a triangular cylinder of 12 wavelength perimeter. The solutions were obtained using ECSR = 1 and $N_{sing} = [(q + 1)/2]$.

An analysis of the local error in the triangular cylinder example shows that as uniform *h*-refinement is applied and the cell sizes are reduced, the error in the corner cells steadily drops. However, the error within the cell next to the corner cell actually begins to grow as that cell gets closer to the corner, and that neighboring cell error dominates the global error measure.

One possible remedy to this situation is to modify the expansion in additional cells near a corner, to better represent the more rapid variation in current density in that region. An alternative remedy is to increase the dimension of the corner cells, relative to the other cells, as suggested by a previous study [6]. This possibility will be investigated in the following.

V. OPTIMUM CORNER CELL DIMENSION

A systematic parameter study was carried out, with the goal of determining the *ECSR* values that minimize the global *NRE*, as a function of q and N_{sing}. The non-corner cell dimensions were fixed at $w_{nc} = q/10\ \lambda$, with the corner cells defined by $w_c = ECSR\ w_{nc}$. Thus, as the order q increases, the cell dimensions increase to maintain a similar number of unknowns. This study considered TM scattering from triangular cylinders, square cylinders, and infinite strips, over a range of sizes. The MFIE was used for the triangular and square cylinders, while the EFIE was used for strips.

Figure 3 shows a plot typical of those generated throughout this investigation. In Fig. 3, the *ECSR* that minimizes the global *NRE* is plotted as a function of q and N_{sing} for the triangular cylinder with perimeter 12 λ. The *ECSR* value is observed to be a rather strong function of both parameters. However, a further study of Fig. 3 yields the observation that the *NRE*-minimizing *ECSR* value for a choice of $N_{sing} = q$ is always near *ECSR* = 2. This observation suggests that the combination of *ECSR* = 2 and $N_{sing} = q$ will generally produce a more accurate result than other values of *ECSR*.

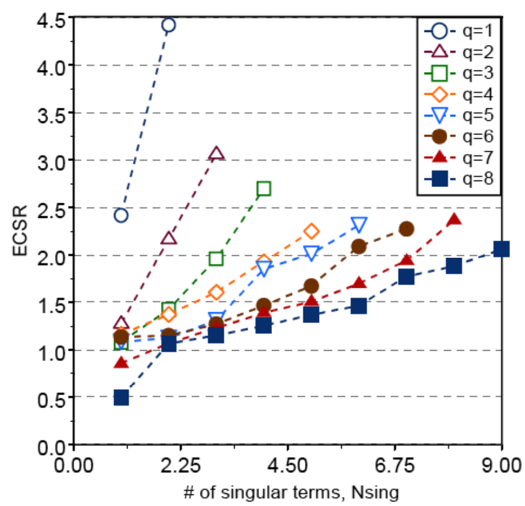

Fig. 3. The ECSR value that minimizes the global *NRE*, as a function of q and N_{sing}. The TM MFIE solutions involve a triangular cylinder of 12 λ perimeter. The non-corner cell size is $w_{nc} = q/10\ \lambda$; the corner cells have dimension $w_c = ECSR\ w_{nc}$.

Figures 4(a) and 4(b) show plots of the global *NRE* and $Slope_q$ versus the degrees of freedom for the same triangular cylinder, obtained from the TM MFIE for *ECSR* = 2 and $N_{sing} = q$. These are improved as compared with Fig. 2, although they still do not offer the ideal behavior of the circular cylinder illustrated by Fig. 1 as *h*-refinement pushes the cell dimensions smaller.

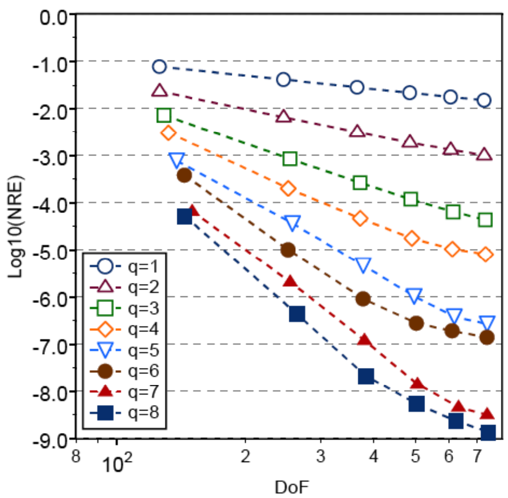

(a)

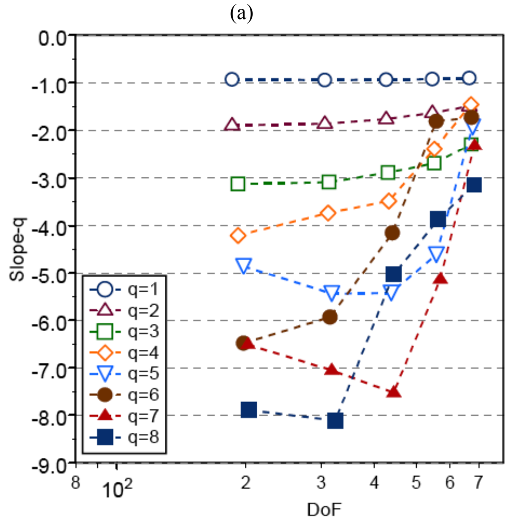

(b)

Fig. 4. (a) Global *NRE* values and (b) $Slope_q$ values for the TM MFIE solutions for a triangular cylinder of 12 wavelength perimeter. The solutions were obtained using ECSR = 2 and $N_{sing} = q$.

Additional parameter studies were carried out, allowing both the non-corner cell dimensions and the ECSR value to vary. One result of that study is shown in Fig. 5, which shows the corner cell dimension that minimizes the global *NRE* versus the non-corner cell dimension, for various values of q with $N_{sing} = q$, for the triangular cylinder used in Figs. 2 and 4. These data indicate that while $ECSR = 2$ is nearly optimal over a wide range of cell sizes, the optimum *ECSR* value generally increases as the cells become small. The data in Fig. 5 are closely tracked by the simple formula,

$$w_c \cong 0.0364 + 1.6723\, w_{nc} + 0.0096q\,. \qquad (7)$$

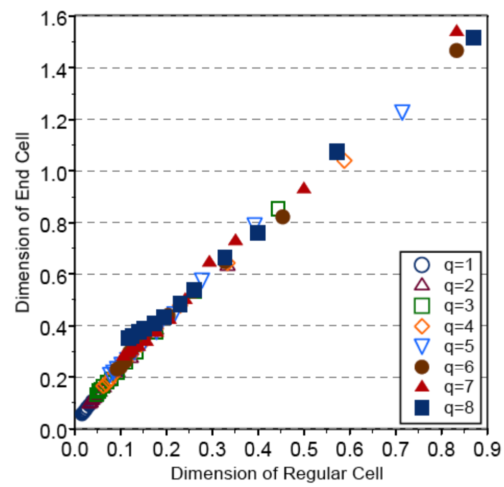

Fig. 5. The corner cell dimension that minimizes the global *NRE* for the TM MFIE solutions for a triangular cylinder of 12 wavelength perimeter. The solutions were obtained using $N_{sing} = q$.

Figures 6(a) and 6(b) show plots of the global *NRE* and $Slope_q$ values versus the degrees of freedom for the triangular cylinder, for $N_{sing} = q$, with each individual result adjusted for the optimum value of *ECSR* corresponding to the results in Fig. 5 (identical results are obtained using the formula in equation (7)). These curves illustrate a much better approximation to the ideal behavior of the circular cylinder, at least for $q \leq 4$. Of course, the identification of the optimal *ECSR* in this manner is not practical for non-canonical targets, and a formula such as equation (7) will vary somewhat from target to target. However, Fig. 6 suggests that a suitable corner cell dimension does exist. Furthermore, it is likely that in the not-too-distant future, some form of adaptive refinement algorithm (perhaps initiated with $ECSR = 2$ and incorporating singular basis functions) should be able to approximate the ideal behavior presented in Fig. 1.

Table 2 summarizes the TM results for several scatterer geometries, including square cylinders and strips, with a range of sizes. Over this range of parameters, it appears that $ECSR = 2$ is a good compromise for q in the range $2 \leq q \leq 8$ and $N_{sing} = q$. Additional studies were carried out for the TE polarization, and lead to similar conclusions as to the optimal *ECSR* value. As an illustration, Figs. 7(a) and 7(b) show plots of the global *NRE* and $Slope_q$ values versus the degrees of freedom for a TE MFIE analysis of the equilateral triangular cylinder with 12 λ perimeter, for $N_{sing} = q$ and $ECSR = 2$.

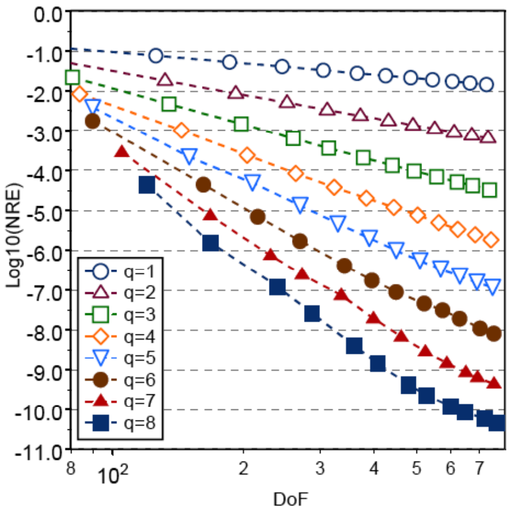

(a)

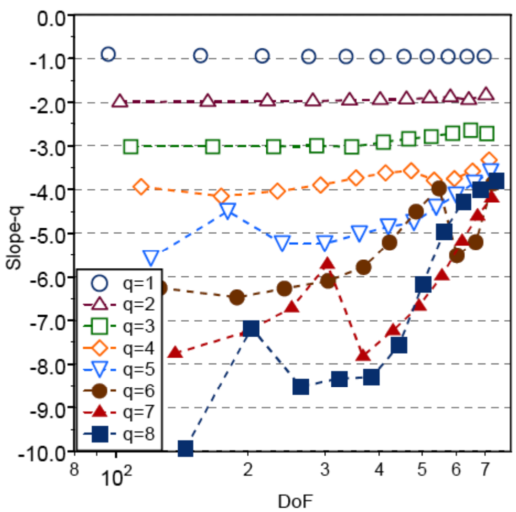

(b)

Fig. 6. (a) Global *NRE* values and (b) $Slope_q$ values for the TM MFIE solutions for a triangular cylinder of 12 wavelength perimeter. The solutions were obtained using optimal ECSR values and $N_{sing} = q$.

Table 2. ECSR that provides the minimum NRE, for models with non-corner cell size = q/10 wavelengths, N_{sing}=q, and the TM polarization.

	Side = 4 wavelengths			Side = 8 wavelengths			Side = 12 wavelengths		
q	Strip	Triangle	Square	Strip	Triangle	Square	Strip	Triangle	Square
1	1.19	2.42	2.59	1.19	2.44	2.15	1.18	2.49	2.03
2	1.74	2.17	1.85	1.67	2.12	1.77	1.64	2.12	1.73
3	1.84	1.96	1.91	1.77	2.02	1.84	1.73	2.03	1.81
4	1.92	1.93	2.03	1.77	1.97	1.93	1.72	1.97	1.89
5	2.00	2.01	2.19	1.87	2.08	2.06	1.81	1.97	2.03
6	2.03	2.09	2.36	1.82	1.77	2.12	1.79	2.01	2.04
7	2.19	1.94	2.67	1.90	1.88	2.20	1.87	1.90	2.12
8	2.27	1.88	2.04	1.97	1.98	2.38	1.90	1.91	2.23

Figures 2, 4, 6, and 7 all involve the triangular cylinder. In these plots, for a constant number of degrees of freedom, as q increases the cell dimensions also increase. Despite the larger cell sizes, the *NRE* is substantially reduced for each increase in q. These curves clearly show the improved accuracy possible with high order basis functions, even for problems that contain an edge singularity.

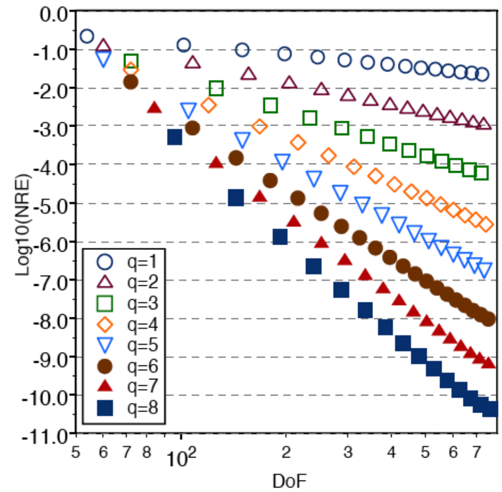

(a)

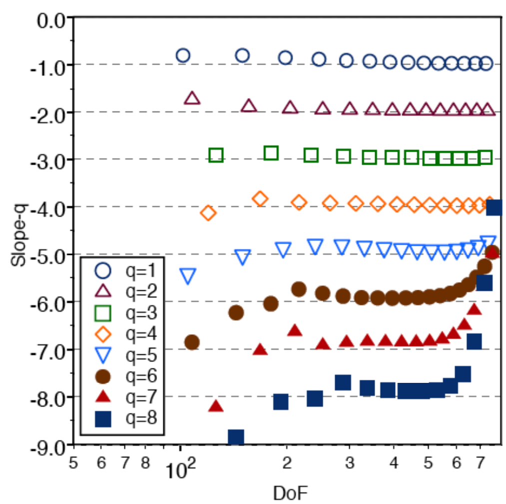

(b)

Fig. 7. (a) Global *NRE* values and (b) $Slope_q$ values for the TE MFIE solutions for a triangular cylinder of 12 wavelength perimeter. The solutions were obtained using ECSR = 2 and $N_{sing} = q$.

VI. CONCLUSIONS

This investigation has shown that the local accuracy of the singular representation used in a corner cell is a function of both the number of singular terms employed in that representation, and the corner cell dimension. If uniform h-refinement is carried too far in an attempt to improve accuracy, the global error will tend to be dominated by the error in cells near (but not immediately adjacent to) the corners, unless the corner cells are not reduced in size to the same extent as the non-corner cells. The parameter studies carried out in this investigation suggest that a fairly optimal combination employs corner cells that are twice the dimension of the non-corner cells (*ECSR* = 2), with an expansion in corner cells that contains a number of singular terms equal to the number of regular terms incorporated within the non-corner cell basis function definition ($N_{sing} = q$). These guidelines should provide a good initial starting point for an electromagnetic analysis of structures containing edges.

REFERENCES

[1] D. R. Wilton and S. Govind, "Incorporation of edge conditions in moment method solutions," *IEEE Trans. Antennas Propagat.*, vol. AP-25, pp. 845-850, 1977.

[2] J. H. Richmond, "On the edge mode in the theory of TM scattering by a strip or strip grating," *IEEE Trans. Antennas Propagat.,* vol. AP-28, pp. 883-887, November 1980.

[3] T. Andersson, "Moment method calculations on apertures using singular basis functions," *IEEE Trans. Antennas Propagat.,* vol. 41, pp. 1709-1716, December 1993.

[4] W. J. Brown and D. R. Wilton, "Singular basis functions and curvilinear triangles in the solution of the electric field integral equation," *IEEE Trans. Antennas Propagat.,* vol. 47, pp. 347-353, February 1999.

[5] R. D. Graglia and G. Lombardi, "Singular higher order complete vector bases for finite methods," *IEEE Trans. Antennas Propagat.*, vol. 52, pp. 1672-1685, July 2004.

[6] D.-K. Sun, L. Vardapetyan, and Z. Cendes, "Two-dimensional curl-conforming singular elements for FEM solutions of dielectric waveguiding structures," *IEEE Trans. Microwave Theory Tech.*, vol. 53, pp. 984-992, March 2005.

[7] M. M. Bibby, A. F. Peterson, and C. M. Coldwell, "High order representations for singular currents at corners," *IEEE Trans. Antennas Propagat.*, vol. 56, pp. 2277-2287, August 2008.

[8] R. F. Harrington, *Time Harmonic Electromagnetic Fields*. New York: McGraw-Hill, 1961, pp. 238-242.

[9] A. F. Peterson, S. L. Ray, and R. Mittra. *Computational Methods for Electromagnetics*. New York: IEEE Press, 1998.

[10] K. J. Bunch and R. W. Grow, "The boundary residual method for three-dimensional homogeneous field problems with boundaries of arbitrary geometries," *International Journal of Infrared and Millimeter Waves*, vol. 10, pp. 1007-1032, 1989.

[11] K. J. Bunch and R. W. Grow, "On the convergence of the method of moments, the boundary residual method, and the point-matching method with a rigorously convergent formulation of the point matching method," *Applied Computational Electromagnetics Society (ACES) J*., vol. 8, pp. 188-202, 1993.

[12] M. M. Bibby and A. F. Peterson, "On the use of over-determined systems in the adaptive numerical solution of integral equations," *IEEE Trans. Antennas Propagat.,* vol. 53, pp. 2267-2273, July 2005.

Malcolm M. Bibby received the B.Eng. and Ph.D. degrees in Electrical Engineering from the University of Liverpool, in 1962 and 1965, respectively, and an MBA from the University of Chicago. He is currently an Adjunct Professor in ECE at Georgia Tech. He has been interested in the numerical aspects associated with antenna design for the last twenty-five years.

Andrew F. Peterson received the B.S., M.S., and Ph.D. degrees in Electrical Engineering from the University of Illinois, Urbana-Champaign in 1982, 1983, and 1986 respectively. Since 1989, he has been a member of the faculty of the School of Electrical and Computer Engineering at the Georgia Institute of Technology, where he is now Professor and Associate Chair for Faculty Development.

Charles M. Coldwell received an A.B. in Mathematics and Ph.D. in Physics from Harvard University, Cambridge, MA, in 1992 and 2002, respectively. He is currently a Senior Software Engineer with Red Hat Inc., Westford, MA, where he specializes in the storage subsystems of the Linux kernel.